www.elsevier.com/locate/ijmecsci

Analytical determination of basic machine-tool settings for generation of spiral bevel gears and compensation of errors of alignment in the cyclo-palloid system

Ignacio Gonzalez-Perez, Alfonso Fuentes-Aznar

PII: S0020-7403(16)30847-5
DOI: http://dx.doi.org/10.1016/j.ijmecsci.2016.11.018
Reference: MS3497

To appear in: *International Journal of Mechanical Sciences*

Received date: 3 August 2016
Revised date: 16 November 2016
Accepted date: 21 November 2016

Cite this article as: Ignacio Gonzalez-Perez and Alfonso Fuentes-Aznar Analytical determination of basic machine-tool settings for generation of spira bevel gears and compensation of errors of alignment in the cyclo-palloid system *International Journal of Mechanical Sciences* http://dx.doi.org/10.1016/j.ijmecsci.2016.11.018

Analytical determination of basic machine-tool settings for generation of spiral bevel gears and compensation of errors of alignment in the cyclo-palloid system

Ignacio Gonzalez-Perez[a], Alfonso Fuentes-Aznar[b]

[a]*Polytechnic University of Cartagena, Department of Mechanical Engineering, Cartagena, Murcia, SPAIN*
[b]*Rochester Institute of Technology, Department of Mechanical Engineering, Rochester, NY, USA*

Abstract

A model for computerized generation of spiral bevel gears in the cyclo-palloid system is proposed. Kinematic conditions of cutting are investigated for tooth thickness and backlash control. Basic machine-tool settings are analytically determined from basic transmission data with the aim of getting favorable conditions of meshing and contact when the gear drive is transmitting a nominal or design load and shaft deflections occur. Errors of alignment of the gear drive due to shaft deflections are considered as input data in the analytical procedure. The proposed procedure is tested through tooth contact and backlash analyses of the gear drive. Several numerical examples are presented.

Keywords: spiral bevel gears, cyclo-palloid system, tooth thickness and backlash control, alignment errors compensation

1. Introduction

Face-hobbing process is widely applied in the industry for generation of spiral and hypoid gears due to its high productivity. Localization of the bearing contact in spiral and hypoid gear drives is a common practice and there are mainly two face-hobbing systems that provide different ways to localize the bearing contact: System (1) is based on the application of a single head-cutter where the cutter tilt angle is used to modify the curvatures of the tooth surfaces, whereas System (2) is based on the application of a dual head-cutter where two separate rotating centers are considered and lead crowning is achieved due to the different cutter radii of inner and outer blades. Processes Spirac©, Spiroflex© and CycloCut© belong to System (1) whereas Cyclo-palloid© belongs to System (2) [1, 2]. While the first system provides more simplicity for machine construction, the second system allows to pay attention just to the head-cutter to localize the bearing contact, regardless of the rest of machine-tool settings that are calculated according to the cutter radii.

Cyclo-palloid system allows conjugated tooth surfaces to be obtained if cutter radii are equal to each other. The basis of cyclo-palloid system can be found in [3]. Lelkes *et al*.[4] explored the possibilities of cyclo-palloid system to localize the bearing contact through lead and profile directions starting from the base of conjugated tooth surfaces. Shih *et al*.[5] proposed an universal hypoid generator mathematical model that includes, among face-milling and face-hobbing methods, the cyclo-palloid system. Later Kawasaki *et al*.[6] investigated conditions of contact and meshing in large-sized spiral bevel gear drives produced through the cyclo-palloid system.

Analytical determination of basic machine-tool settings from basic transmission data was successfully applied to face-milled and face-hobbed spiral and hypoid gears in [7] for determination of the gear member following Standard ANSI/AGMA 2005-C96 [8] and considering System (1) as a generating or as a non-generated process. Then, an algorithm for the synthesis of the pinion is required to obtain favorable conditions of meshing and contact, as the ones illustrated in [9, 10, 11, 12, 13] for spiral bevel and hypoid gears. The simplicity of the cyclo-palloid system for obtention of conjugated tooth surfaces in spiral bevel gears allows analytical determination of basic machine-tool settings to be obtained not only for the gear, but also for the pinion, following the mentioned standard. Then, application of similar ideas for localization of the bearing contact to those shown in [4] allows the formation of the bearing contact to be controlled in a spiral bevel gear drive.

Since errors of alignment caused by shaft deflections may affect considerably to the conditions of meshing and contact, machine-tool settings need to be accordingly corrected. A method for machine-tool settings correction was

proposed in [14] to compensate manufacturing errors in the cyclo-palloid system. In the present paper, an analytical method for machine-tool settings correction in order to compensate errors of alignment due to shaft deflections is proposed. Procedures for compensation of shafts deflections have been proposed in [15] for spur gear drives and in [16] for spiral bevel gears generated by face-milling.

The main goals of research in this paper are summarized as follows:

(i) Computerized generation of the tooth surfaces of a spiral bevel gear drive considering the cyclo-palloid system and establishment of the kinematic conditions of cutting for tooth thickness and backlash control.

(ii) Analytical determination of basic machine-tool setting from basic transmission data for spiral bevel gears produced through the cyclo-palloid system.

(iii) Analytical correction of machine-tool settings to compensate errors of alignment caused by shaft deflections.

(iv) Application of localization of the bearing contact for observation of favorable conditions of meshing and contact for the design load.

Tooth contact and backlash analyses are considered to prove the goodness of the proposed ideas. Several numerical examples are presented.

2. Computerized generation of spiral bevel gears through the cyclo-palloid system

The cyclo-palloid system is based on the application of a dual face-hobbing cutter as the one that is shown in Fig. 1. Here, two separate disks with rotating axes $\mathbf{a}_i$ and $\mathbf{a}_o$ are considered. The inner blades are attached to the disk with rotation axis $\mathbf{a}_i$ whereas the outer blades are attached to the disk with rotation axis $\mathbf{a}_o$.

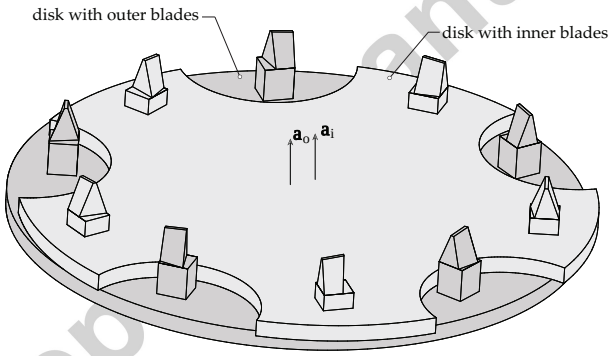

Figure 1: Dual face-hobbing cutter for generation of a right-hand gear.

The main aspects of the geometry of the blades of a dual face-hobbing cutter are similar to those already described for a face-hobbing cutter in [17, 18, 19]. However, details of the geometry of the blades are exposed here for a major clarity of the considered variables to control the contact pattern, as it will be shown in Section 5.

2.1. Geometry of the blades

Figure 2 shows several geometries for a inner blade and the coordinate systems S_a and S_b for the definition of the cutting edge. Their origins are located at reference point P_i. Definition of the cutting edge for an outer blade is similar and it is not included here for the purpose of simplicity. Profile pressure angle α_i (measured on the front plane) is related to blade pressure angle α_{ib} through relation (see [7]):

$$\tan\alpha_i \cdot \cos\alpha_{ir} = \tan\alpha_{ib} \tag{1}$$

Here, α_{ir} is the rake angle. System S_b results from the rotation of system S_a around axis y_a the value α_{ir}. Blade pressure angle α_{ib} is defined in plane $x_b y_b$.

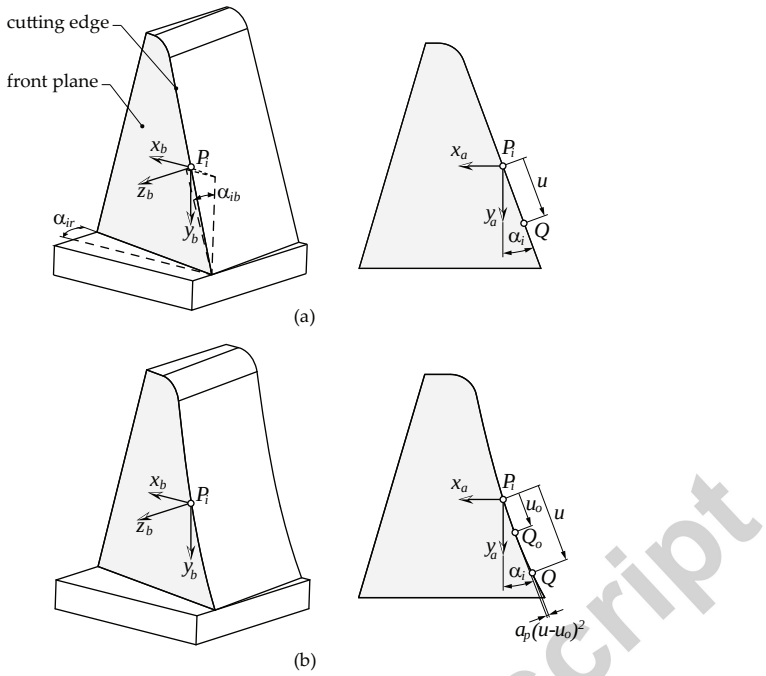

Figure 2: Geometries of a inner blade with (a) straight profile and (b) parabolic profile.

Position vector of point Q of the cutting edge is defined in system S_a as

$$\mathbf{r}_a^{(Q)} = \begin{bmatrix} -u\sin\alpha_i - a_p(u-u_o)^2\cos\alpha_i \\ +u\cos\alpha_i - a_p(u-u_o)^2\sin\alpha_i \\ 0 \\ 1 \end{bmatrix} \tag{2}$$

Here, a_p is the parabola coefficient and u_o locates the apex of the parabola Q_o. A straight profile may be derived considering $a_p = 0$. Parameter u_o may be useful to shift the bearing contact in profile direction.

Other profile definitions [19] are also possible as those based on circular arcs, those based on application of top rem for root relief of the gear tooth, or those based on application of tip relief.

Finally, the cutting edge can be obtained in system S_b by coordinate transformation

$$\mathbf{r}_b^{(Q)} = \mathbf{M}_{ba}\mathbf{r}_a^{(Q)} \tag{3}$$

Here, $\mathbf{M}_{ba}$ is a 4×4 matrix given as

$$\mathbf{M}_{ba} = \begin{bmatrix} \cos\alpha_{ir} & 0 & \sin\alpha_{ir} & 0 \\ 0 & 1 & 0 & 0 \\ -\sin\alpha_{ir} & 0 & \cos\alpha_{ir} & 0 \\ 0 & 0 & 0 & 1 \end{bmatrix} \tag{4}$$

Additional rotations to consider hook angle of the blades can be also applied as it is illustrated in [18, 19].

2.2. Geometry of the cutter

Figure 3 shows a schematic representation of a cyclo-palloid cutter where just two blades are installed. Here, cutter radii r_{ci} and r_{co} for the inner and the outer blades are exaggeratedly different for the purpose of a better clarity in the representation. Reference points P_i and P_o describe circular trajectories about centers O_{ci} and O_{co}, respectively. Such trajectories are exclusively due to the rotations of both disks of the dual face-hobbing cutter on the cradle, not

represented in Fig. 3. Both blades are usually assembled considering that axes x_{bi} and x_{bo} are aligned with lines that are in tangency with circles c_i and c_o at points T_i and T_o, respectively. The radii for such circles, ρ_i and ρ_o, are determined as

$$\rho_i = \rho_o = \frac{m_b N_b}{2} \tag{5}$$

Here, m_b is the blade module and N_b is the number of blade groups.

The assembly angles δ_i and δ_o are then given as

$$\delta_k = \arcsin \frac{\rho_k}{r_{ck}}, \quad k = i, o \tag{6}$$

Figure 3 shows that point P'_o represents the position of point P_o when it passes through point P_i. In such situation, axis x_{bo} will be aligned with axis x_{bi} and both axes will be in tangency with circles c_i and c_o at points T_i and T'_o, respectively. Coordinate transformation from system S_{bk} to system S_{ck}, $k = (i, o)$, allows the cutting edge to be defined in system S_{ck}.

$$\mathbf{r}_c^{(Q)} = \mathbf{M}_{cb}\mathbf{r}_b^{(Q)} \tag{7}$$

Here, subscript k is suppressed for a major clarity.

Matrix M_{cb} is given as

$$\mathbf{M}_{cb} = \begin{bmatrix} \cos\delta_k & 0 & -\sin\delta_k & r_{ck} \\ 0 & 1 & 0 & 0 \\ \sin\delta_k & 0 & \cos\delta_k & 0 \\ 0 & 0 & 0 & 1 \end{bmatrix}, \quad k = i, o \tag{8}$$

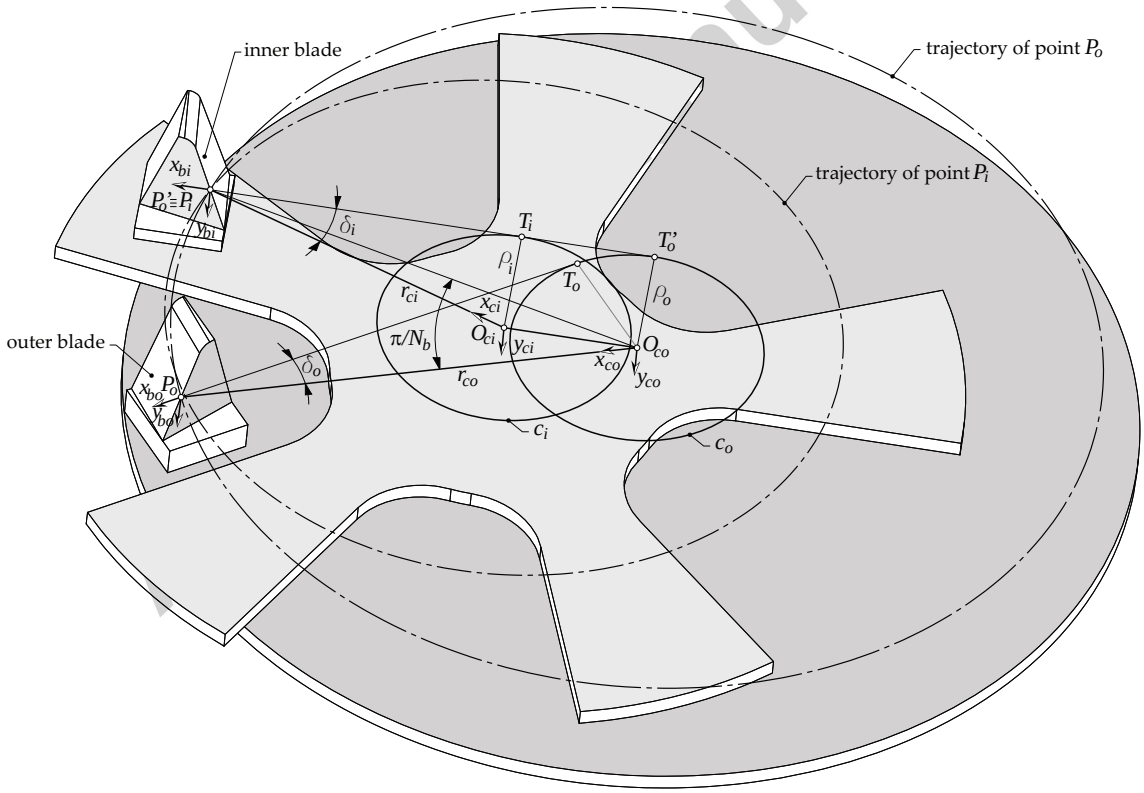

Figure 3: Schematic representation of the geometry of a cyclo-palloid cutter.

2.3. Settings of cutter and gear

Both, cutter and gear, are installed in the cutting machine considering a coordinate system S_m that is attached to the frame. Figure 4 illustrates the kinematic operation of the blades in system S_m. Points O_{ci}, O_{co} and $P_i \equiv P'_o$ are positioned in coordinate system S_m. Two magnitudes of the gear are represented here, the mean cone distance A_m, that is equal to $\overline{O_m P_i}$, and the mean spiral angle ψ_m. The positioning of the gear will be illustrated below.

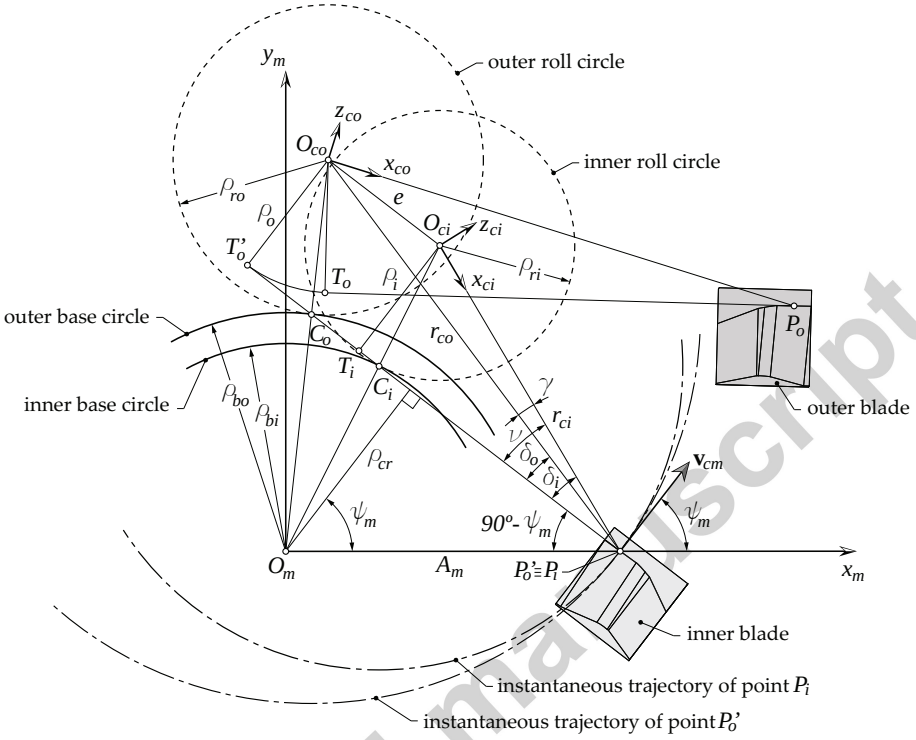

Figure 4: Kinematic operation of the blades in coordinate system S_m for a right-hand gear.

The cutter disks are carried out by a cradle (not represented in Fig. 4) that rotates around an axis that is perpendicular to plane $x_m y_m$ and passes through point O_m. The relative velocities of points P_i and P'_o respect to the machine frame are represented by vector $\mathbf{v}_{cm}$ that makes angle ψ_m with axis x_m. The line that is perpendicular to vector $\mathbf{v}_{cm}$ forms the so-called slope angle ν respect to segment $\overline{O_{ci}P_i}$. Such a line is aligned with segments $\overline{P_i T_i}$ and $\overline{P'_o T'_o}$. The intersections of such a line with segments $\overline{O_m O_{ci}}$ and $\overline{O_m O_{co}}$ allows instantaneous centers of rotations C_i and C_o of the motions of the cutter disks respect to the machine frame to be determined. The instantaneous trajectories of points P_i and P'_o about points C_i and C_o are illustrated as well in Fig. 4. The common tangent to such trajectories at point $P_i \equiv P'_o$ coincides with vector $\mathbf{v}_{cm}$. Points C_i and C_o allows the roll and base circles of the relative motions of the blades respect to the frame to be determined.

The slope angle ν is given as

$$\nu = \arcsin \frac{\rho_i}{r_{ci}} = \arcsin \frac{m_b N_b}{2 r_{ci}} \tag{9}$$

The eccentricity e is then derived as

$$e = \sqrt{r_{co}^2 - r_{ci}^2 \sin^2 \nu} - r_{ci} \cos \nu \tag{10}$$

Definition of assembly angles δ_i and δ_o according to Eq. (6) implies that

$$\delta_i = \nu, \quad \delta_o = \nu - \gamma \tag{11}$$

although this is not mandatory (Eq. (6) is also not mandatory). Here, γ is an auxiliar angle defined as

$$\gamma = \arcsin \frac{e \sin \nu}{r_{co}} \tag{12}$$

Figure 5 shows the assembly of the cutter and the gear in coordinate system S_m. Center O_{ci} (respectively, O_{co}) is positioned through the machine distance for the inner blades M_{di} (respectively, the machine distance for the outer blades M_{do}) and the cradle angle q_{2i} (respectively, q_{2o}) and are given as follows

$$M_{dk} = \sqrt{A_m^2 + r_{ck}^2 - 2A_m r_{ck} \sin(\psi_m - \nu_k)}, \quad k = (i, o) \tag{13}$$

$$q_{2k} = \arcsin \left[\frac{r_{ck}}{M_{dk}} \cos(\psi_m - \nu_k) \right], \quad k = (i, o) \tag{14}$$

with $\nu_i = \nu$ and $\nu_o = \nu - \gamma$.

On the other hand, the gear is positioned with the apex of the pitch cone at point O_m whereas the pitch cone axis forms the pitch angle γ_g with axis x_m.

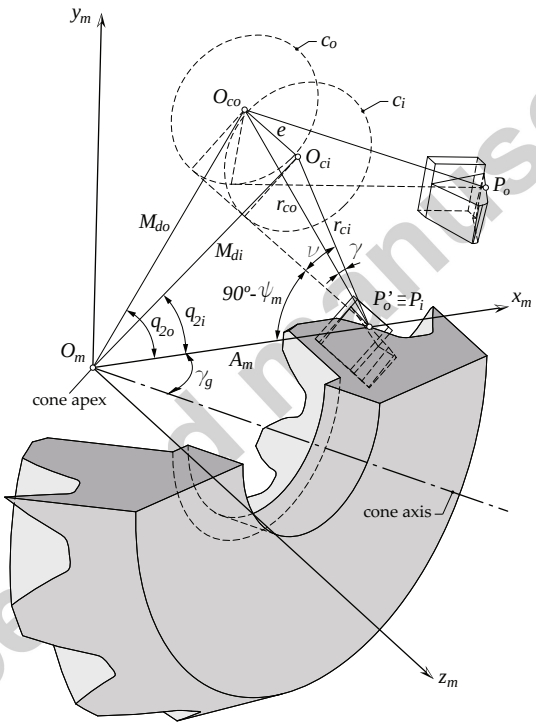

Figure 5: Assembly of cutter and gear in coordinate system S_m for a right-hand gear.

2.4. Computerized generation of the gear

Figure 6 shows the applied coordinate systems for computation of gear tooth surfaces. Here, rotations of the cutter disks are considered through magnitudes θ_i and θ_o. Auxiliar coordinate systems $S_{ci'}$ and $S_{co'}$ are considered for coordinate transformation from systems S_{ci} and S_{co} that are attached to the blades.

$$\mathbf{r}_{ck'}(u, \theta_k) = \mathbf{M}_{ck',ck}(\theta_k)\mathbf{r}_{ck}(u), \quad k = (i, o) \tag{15}$$

Here, $\mathbf{M}_{ck',ck}(\theta_k)$ is a 4×4 matrix given as

$$\mathbf{M}_{ck',ck} = \begin{bmatrix} \cos\theta_k & 0 & -\sin\theta_k & 0 \\ 0 & 1 & 0 & 0 \\ \sin\theta_k & 0 & \cos\theta_k & 0 \\ 0 & 0 & 0 & 1 \end{bmatrix}, \quad k = (i, o) \tag{16}$$

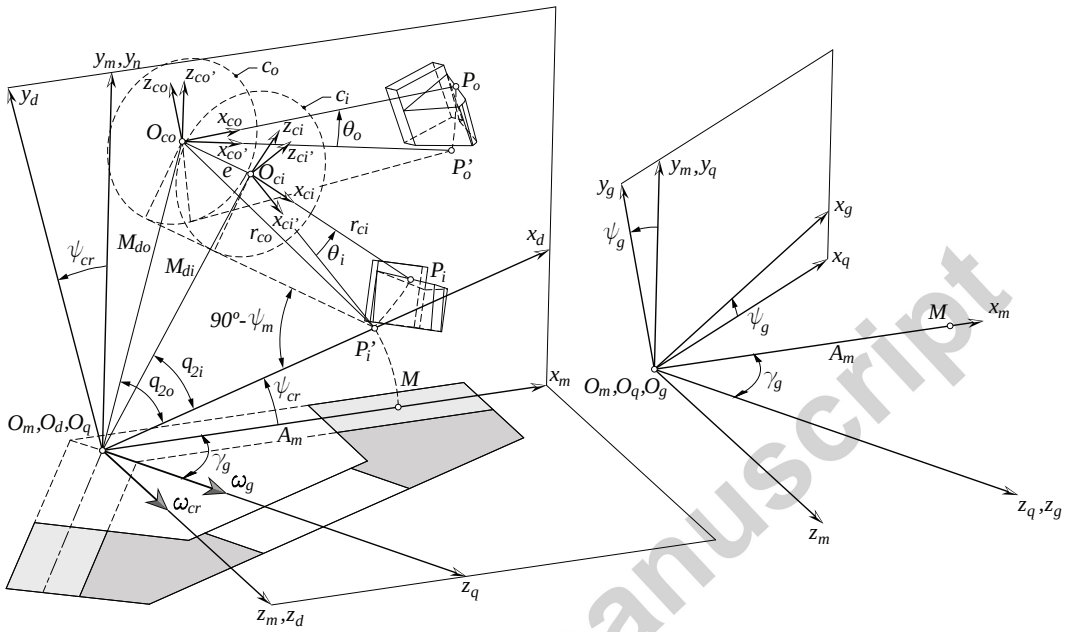

Figure 6: Applied coordinate systems for computerized generation of a right-hand gear.

Coordinate system S_d is attached to the cradle and rotates the magnitude ψ_{cr} respect to system S_m. Coordinate transformation from system $S_{ck'}$ to system S_m is given as

$$\mathbf{r}_m(u, \theta_k, \psi_{cr}) = \mathbf{M}_{md}(\psi_{cr})\mathbf{M}_{d,ck'}\mathbf{r}_{ck'}(u, \theta_k), \quad k = (i, o) \tag{17}$$

Here,

$$\mathbf{M}_{md} = \begin{bmatrix} \cos\psi_{cr} & -\sin\psi_{cr} & 0 & 0 \\ \sin\psi_{cr} & \cos\psi_{cr} & 0 & 0 \\ 0 & 0 & 1 & 0 \\ 0 & 0 & 0 & 1 \end{bmatrix} \tag{18}$$

$$\mathbf{M}_{d,ck'} = \begin{bmatrix} \sin(\psi_m - \nu_k) & 0 & \cos(\psi_m - \nu_k) & M_{dk}\cos q_{2k} \\ -\cos(\psi_m - \nu_k) & 0 & \sin(\psi_m - \nu_k) & M_{dk}\sin q_{2k} \\ 0 & -1 & 0 & 0 \\ 0 & 0 & 0 & 1 \end{bmatrix}, \quad k = (i, o) \tag{19}$$

with $\nu_i = \nu$ and $\nu_o = \nu - \gamma$.

Finally, coordinate transformation from system S_m to system S_g attached to the gear is given as

$$\mathbf{r}_g(u, \theta_k, \psi_{cr}, \psi_g(\theta_k, \psi_{cr})) = \mathbf{M}_{gq}(\psi_g)\mathbf{M}_{qm}\mathbf{r}_m(u, \theta_k, \psi_{cr}) \tag{20}$$

Here,

$$\mathbf{M}_{gq} = \begin{bmatrix} \cos\psi_g & \sin\psi_g & 0 & 0 \\ -\sin\psi_g & \cos\psi_g & 0 & 0 \\ 0 & 0 & 1 & 0 \\ 0 & 0 & 0 & 1 \end{bmatrix} \tag{21}$$

$$\mathbf{M}_{qm} = \begin{bmatrix} \sin\gamma_g & 0 & -\cos\gamma_g & 0 \\ 0 & 1 & 0 & 0 \\ \cos\gamma_g & 0 & \sin\gamma_g & 0 \\ 0 & 0 & 0 & 1 \end{bmatrix} \tag{22}$$

$$\psi_g = m_{gc} \cdot \psi_{cr} - m_{gb} \cdot \theta_k, \quad k = (i, o) \tag{23}$$

Here, m_{gc} is the ratio of gear-to-cradle roll (known as the ratio of gear roll or velocity ratio) and m_{gb} is the ratio of gear-to-blade roll. The ratio of gear roll is derived considering the relation between the linear velocities of the cradle and the gear at pitch point M

$$\omega_{cr} A_m = \omega_g A_m \sin\gamma_g \tag{24}$$

$$m_{gc} = \frac{\omega_g}{\omega_{cr}} = \frac{1}{\sin\gamma_g} \tag{25}$$

The ratio of gear-to-blade roll is given as

$$m_{gb} = \left(\frac{\psi_g}{\psi_{cr}}\right) \cdot \left(\frac{\psi_{cr}}{\theta_k}\right), \quad k = (i, o) \tag{26}$$

Here,

$$\left(\frac{\psi_g}{\psi_{cr}}\right) = \frac{1}{\sin\gamma_g} = \frac{N_c}{N_g} \tag{27}$$

where N_c can be considered as the number of teeth of a crown gear that rotates rigidly connected to the cradle and N_g is the gear tooth number. On the other hand,

$$\left(\frac{\psi_{cr}}{\theta_k}\right) = \frac{\rho_{rk}}{\rho_{bk}}, \quad k = (i, o) \tag{28}$$

where ρ_{rk} and ρ_{bk} are the radii of roll and base circles, respectively (see Fig. 4). The relation between such radii satisfies the relation

$$\frac{\rho_{rk}}{\rho_{bk}} = \frac{\rho_k}{\rho_{cr}} = \frac{(m_b N_b)/2}{(m_b N_c)/2} = \frac{N_b}{N_c}, \quad k = (i, o) \tag{29}$$

where ρ_k was already defined (see Eq. (5)) and ρ_{cr} (see Fig. 4) can be considered as the crown gear radius. Finally, the ratio of gear-to-blade roll gives

$$m_{gb} = \frac{N_c}{N_g} \cdot \frac{N_b}{N_c} = \frac{N_b}{N_g} \tag{30}$$

Simultaneous consideration of Eq. (20) and the equation of meshing

$$\left(\frac{\partial \mathbf{r}_g}{\partial u} \times \frac{\partial \mathbf{r}_g}{\partial \theta_k}\right) \cdot \frac{\partial \mathbf{r}_g}{\partial \psi_{cr}} = 0 \tag{31}$$

allows the gear tooth surfaces to be determined [20].

2.5. Variation of the slope angle for tooth thickness control

The variation of the slope angle ν (see Fig. 4) allows the kinematic operation of the blades to be changed in order to modify the tooth thickness of the gear tooth and, consequently, to control the backlash at the gear drive while keeping freedom in the selection of the cutting radii r_{ci} and r_{co} for localization of the bearing contact.

The ratio of gear-to-blade roll can be defined considering the slope angle ν (see Fig. 4)

$$m_{gb} = \left(\frac{\psi_g}{\psi_{cr}}\right) \cdot \left(\frac{\psi_{cr}}{\theta_k}\right) = \frac{1}{\sin\gamma_g} \cdot \frac{\rho_k}{\rho_{cr}} = \frac{1}{\sin\gamma_g} \cdot \frac{r_{ck} \sin\nu_k}{A_m \cos\psi_m}, \quad k = (i, o) \tag{32}$$

with $\nu_i = \nu$ and $\nu_o = \nu - \gamma$.

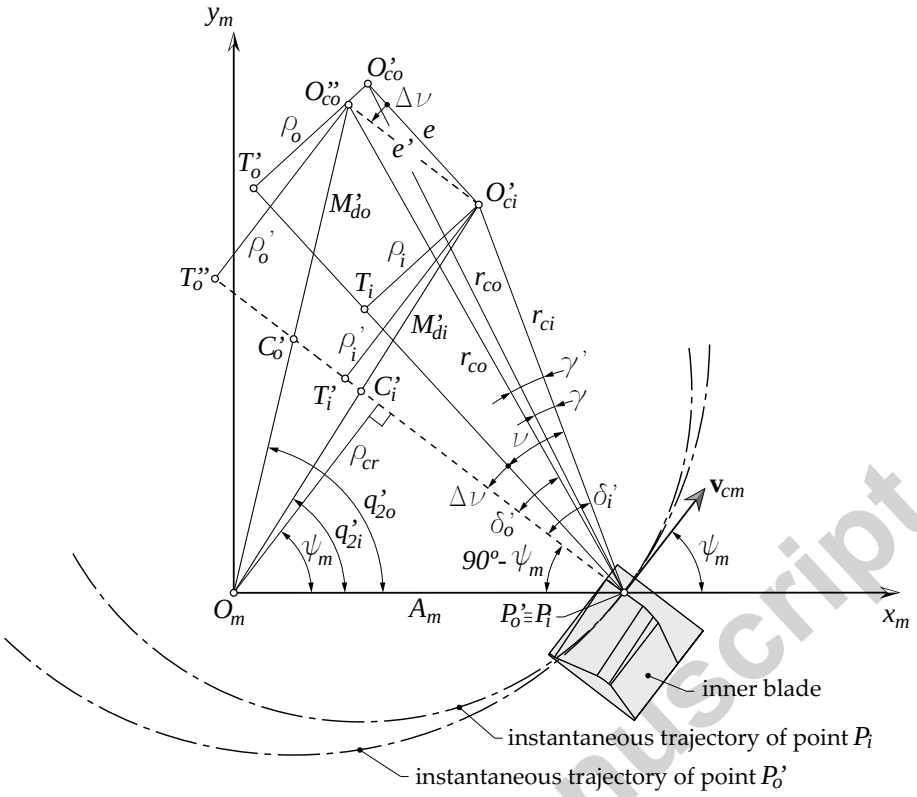

Figure 7: Application of an additional slope angle $\Delta\nu$.

Figure 7 shows the effects of an additional slope angle $\Delta\nu$ on the kinematic operation of the blades and on the machine-tool settings for the cutter. The additional slope angle $\Delta\nu$ modifies the radii of the roll circles that are set now to ρ'_i and ρ'_o, while the radius ρ_{cr} is kept constant. The new eccentricity e' is given now as

$$e' = \sqrt{r_{co}^2 - r_{ci}^2 \sin^2(\nu + \Delta\nu)} - r_{ci}\cos(\nu + \Delta\nu) \tag{33}$$

The new machine distances and cradle angles are given then as

$$M'_{dk} = \sqrt{A_m^2 + r_{ck}^2 - 2A_m r_{ck}\sin(\psi_m - \nu'_k)}, \quad k = (i, o) \tag{34}$$

$$q'_{2k} = \arcsin\left[\frac{r_{ck}}{M'_{dk}}\cos(\psi_m - \nu'_k)\right], \quad k = (i, o) \tag{35}$$

with $\nu'_i = \nu + \Delta\nu$ and $\nu'_o = \nu + \Delta\nu - \gamma'$. Here,

$$\gamma' = \arcsin\frac{e'\sin(\nu + \Delta\nu)}{r_{co}} \tag{36}$$

The new gear-to-blade roll is given now as

$$m'_{gb} = \frac{1}{\sin\gamma_g}\cdot\frac{\rho'_k}{\rho_{cr}} = \frac{1}{\sin\gamma_g}\cdot\frac{r_{ck}\sin\nu'_k}{A_m\cos\psi_m}, \quad k = (i, o) \tag{37}$$

Since $\rho'_i = \rho'_o$, the same ratio of gear-to-blade roll is obtained for inner and outer blades.

The assembly angles δ'_i and δ'_o can be set as

$$\delta'_i = \nu + \Delta\nu, \quad \delta'_o = \nu + \Delta\nu - \gamma' \tag{38}$$

The effects of the additional slope angle $\Delta\nu$ will be shown in Section 5.

3. Analytical determination of pinion and gear basic machine-tool settings from blank data

The blank data of a spiral bevel gear drive are those data that allow a complete definition of the layout of the gear drive. Such data were derived in [15] for spiral bevel and hypoid gears produced either by face-milling or face-hobbing. Determination of blank data from basic data such as the power to transmit, the gear ratio, the pinion speed, the shaft angle, and the quality of gears, can be based as well on the application of Standard ANSI/AGMA 2005-C96 [8] for the case of spiral bevel gears produced through the cyclo-palloid system. Once that the blank data are determined, basic machine-tool settings can be easily derived for pinion and gear considering, initially, conjugated action and zero backlash.

Inner and outer cutter radii can be set as $r_{ci} = r_{co} = r_c$, where r_c is the mean cutter radius that is selected according to Standard ANSI/AGMA 2005-C96 among the available tools. Since the mean normal module m_{mn} is also determined among the blank data following the mentioned standard, the blade module m_b can be set as $m_b = m_{mn}$ and the slope angle ν can be determined from Eq. (9). The mean cone distance A_m, the mean spiral angle ψ_m, and the gear tooth number N_g, $g = (1, 2)$, are also blank data. Here, subindex 1 is applied to the pinion and subindex 2 is applied to the gear. Machine distances, cradle angles, gear-to-cradle ratios, and gear-to-blade ratios, are then determined according to Eqs. (13), (14), (25), (30), respectively, either for the pinion or the gear.

Regarding the position of the pinion (or the gear) in the cutting machine, the basic machine-tool settings are set as follows (see [15] to identify nomenclature and settings):

- Machine root angles $\gamma_{m1} = \gamma_1$, $\gamma_{m2} = \gamma_2$, where γ_g, $g = (1, 2)$, are the pitch angles.
- Blank offsets $\Delta E_{m1} = 0$, $\Delta E_{m2} = 0$.
- Sliding bases $\Delta X_{B1} = 0$, $\Delta X_{B2} = 0$.
- Machine centers to back $\Delta X_{D1} = 0$, $\Delta X_{D2} = 0$.

These settings correspond to the position that is illustrated in Fig. 5 for a right-hand gear.

Pinion and gear mean normal chordal addendums, a_{c1} and a_{c2}, and pinion and gear mean normal chordal tooth thicknesses, t_{n1} and t_{n2}, can also be derived from application of the mentioned standard for observation of a given backlash. Here, application of an additional slope angle $\Delta\nu$ according to Subsection 2.5 is very important since it will allow tooth thicknesses to be modified and contact conditions to be kept.

Figure 8 shows points M_i and M_o of the gear tooth surfaces that belong to a normal plane $x_n y_n$ that passes through the pitch point M whereas its normal axis z_n forms the angle ψ_m with longitudinal axis z_k. The distance between points M_i and M_o is given by t_{ng}, $g = (1, 2)$. Both points are at a distance a_{cg}, $g = (1, 2)$, from the tip. Both points can be set by coordinate transformation from system S_g to system S_n as follows

$$\mathbf{r}_n^{(M_i)}(u^{(M_i)}, \theta_i^{(M_i)}, \psi_{cr}^{(M_i)}, \Delta\nu_g, \phi_g) = \mathbf{M}_{ng}(\phi_g) \cdot \mathbf{r}_g^{(M_i)}(u^{(M_i)}, \theta_i^{(M_i)}, \psi_{cr}^{(M_i)}, \Delta\nu_g) \tag{39}$$

$$\mathbf{r}_n^{(M_o)}(u^{(M_o)}, \theta_o^{(M_o)}, \psi_{cr}^{(M_o)}, \Delta\nu_g, \phi_g) = \mathbf{M}_{ng}(\phi_g) \cdot \mathbf{r}_g^{(M_o)}(u^{(M_o)}, \theta_o^{(M_o)}, \psi_{cr}^{(M_o)}, \Delta\nu_g) \tag{40}$$

Here, $\Delta\nu_g$ is the required additional slope angle to get t_{ng}, and ϕ_g is the required angle of rotation of the gear to get points M_i and M_o at the positions illustrated in Fig. 8. Vector $\mathbf{r}_g$ is obtained considering the machine-tool settings derived in Subsection 2.5 to take into account $\Delta\nu_g$, $g = (1, 2)$. $\mathbf{M}_{ng}$ is a 4×4 matrix for coordinate transformation from system S_g to system S_n.

A total of eight unknowns $\{u^{(M_i)}, \theta_i^{(M_i)}, \psi_{cr}^{(M_i)}, u^{(M_o)}, \theta_o^{(M_o)}, \psi_{cr}^{(M_o)}, \Delta\nu_g, \phi_g\}$ are to-be-obtained. The problem requires eight equations to be numerically solved by using, for example, the Newton-Raphson method [21]. The eight condi-

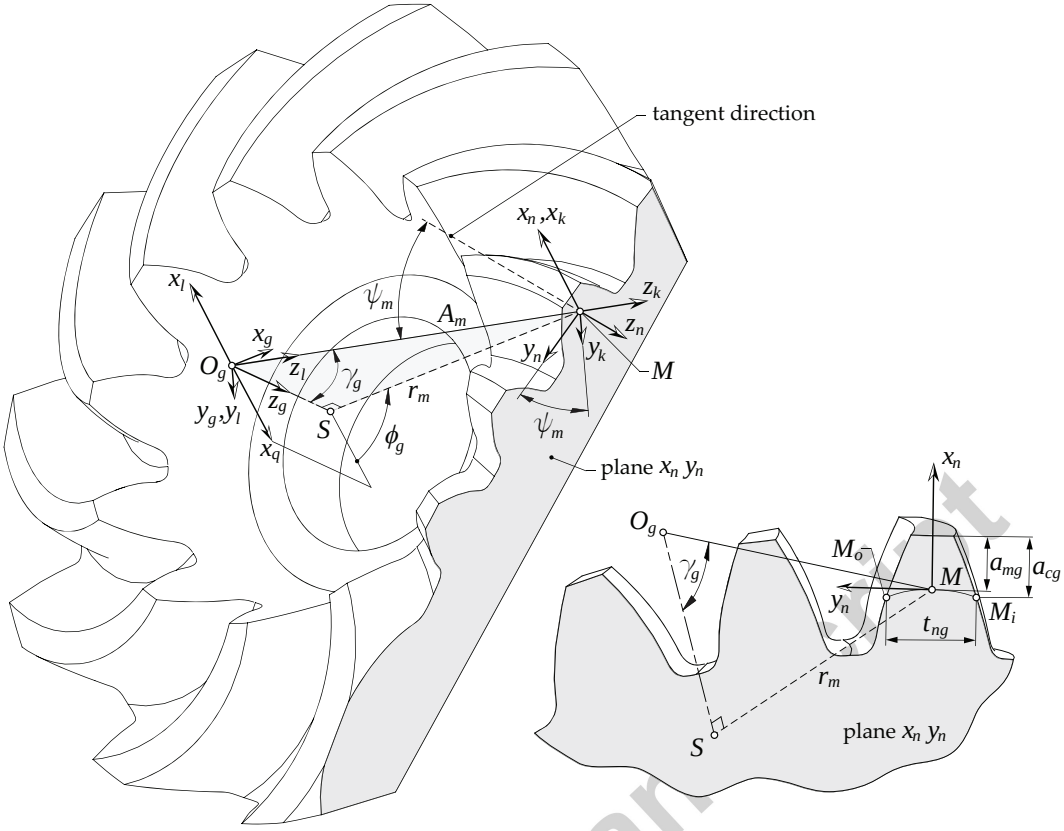

Figure 8: For determination of normal chordal tooth thickness t_{ng}.

tions are as follows:

$$f_i(u^{(M_i)}, \theta_i^{(M_i)}, \psi_{cr}^{(M_i)}, \Delta\nu_g) = 0 \quad (41)$$

$$f_o(u^{(M_o)}, \theta_o^{(M_o)}, \psi_{cr}^{(M_o)}, \Delta\nu_g) = 0 \quad (42)$$

$$r_{nx}^{(M_i)} - (a_{mg} - a_{cg}) = 0 \quad (43)$$

$$r_{ny}^{(M_i)} - \left(\mp\frac{t_{ng}}{2}\right) = 0 \quad (44)$$

$$r_{nz}^{(M_i)} = 0 \quad (45)$$

$$r_{nx}^{(M_o)} - (a_{mg} - a_{cg}) = 0 \quad (46)$$

$$r_{ny}^{(M_o)} - \left(\pm\frac{t_{ng}}{2}\right) = 0 \quad (47)$$

$$r_{nz}^{(M_o)} = 0 \quad (48)$$

Here, $f_i = 0$ and $f_o = 0$ are the corresponding equations of meshing for points M_i and M_o, and a_{mg} is the gear mean addendum (another blank data). The upper sign is considered for a right-hand gear whereas the lower sign is for a left-hand gear. The problem is solved twice, for pinion and gear, obtaining the additional slope angles $\Delta\nu_1$ and $\Delta\nu_2$ for observation of tooth thicknesses t_{n1} and t_{n2}.

4. Corrections of machine-tool settings for compensation of errors of alignment

Errors of alignment due to shaft deflections may be obtained by stress analysis of a gear drive where the shafts are included into the finite element model. Examples of determination of errors of alignment due to shaft deflections in

spiral bevel gear drives can be found in [16]. Such errors are obtained for a design load (a torque). Figure 9 shows the alignment errors exaggeratedly large for a better illustration. Errors are defined in a fixed coordinate system S_f as pinion axial error ΔA_1, wheel axial error ΔA_2, shaft angle error $\Delta\gamma$, and shortest center distance error ΔE.

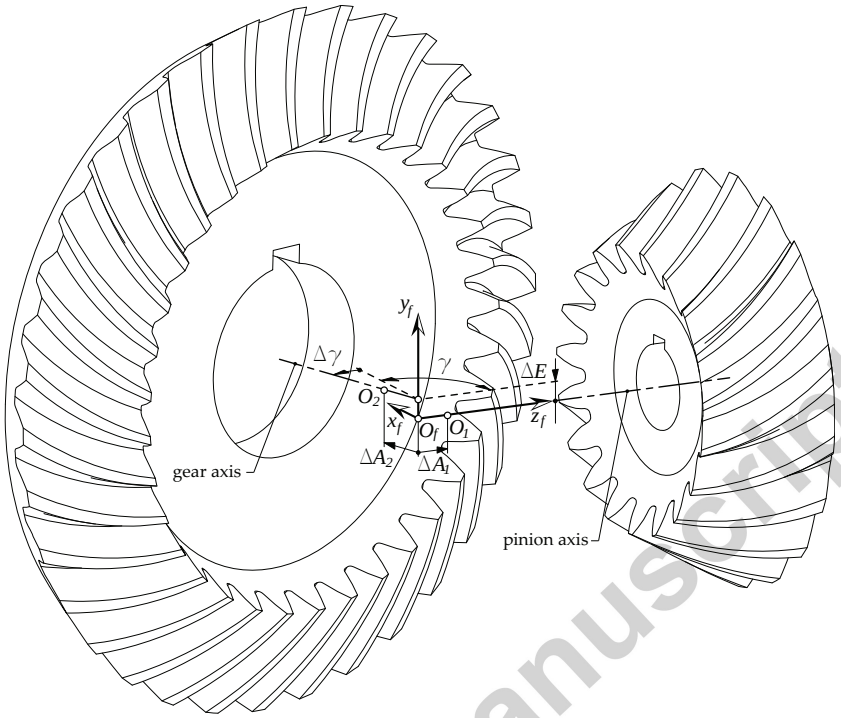

Figure 9: Illustration of errors of alignment in a spiral bevel gear drive.

Compensation of errors of alignment in spiral bevel gears produced through the cyclo-palloid system may be provided by determination of basic machine-tool settings at the design stage. Figure 10 shows again the errors of alignment defined in the fixed coordinate system S_f. Additionally, fixed machine coordinate systems S_{m1} and S_{m2} are included to illustrate how pinion and gear will be set in the cutting machine, respectively. Pinion and gear are represented by means of their layouts. Here, pitch points M_1 and M_2 of pinion and gear, respectively, coincide at point M if no errors of alignment occur.

Knowing in advance the errors of alignment though the procedure exposed in [16], it will be possible to redesign the gear drive for compensation of such errors. Existence of a shaft angle error $\Delta\gamma$ implies that a gear drive with a shaft angle of $\gamma + \Delta\gamma$ has to be redesigned. Determination of the axodes or pitch cones of the new gear drive may be performed considering axis $O_m M$ as the new instantaneous axis of rotation between pinion and gear [20]. This provides auxiliary pitch angles γ_1' and γ_2'

$$\gamma_1' = \arctan \frac{\sin(\gamma + \Delta\gamma)}{m_{12} + \cos(\gamma + \Delta\gamma)} \tag{49}$$

$$\gamma_2' = \arctan \frac{\sin(\gamma + \Delta\gamma)}{m_{21} + \cos(\gamma + \Delta\gamma)} \tag{50}$$

Here, $m_{12} = 1/m_{21} = N_2/N_1$ is the gear ratio. The auxiliary pitch angles γ_1' and γ_2' are considered for determination of basic-machine tool settings, but not for the modification of the pitch angles of pinion and gear.

New machine root angles γ_{m1}' and γ_{m2}' are then set to

$$\gamma_{m1}' = \gamma_1' \tag{51}$$

$$\gamma_{m2}' = \gamma_2' \tag{52}$$

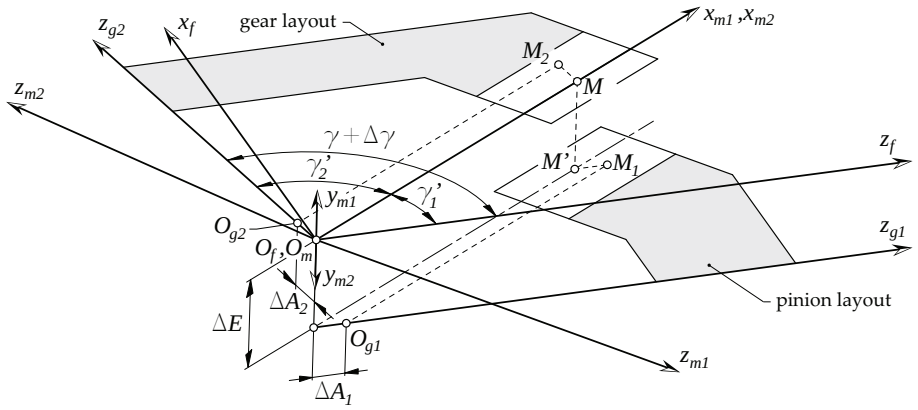

Figure 10: For compensation of errors of alignment.

On the other hand, gear-to-cradle rolls are set to

$$m'_{1c} = \frac{1}{\sin\gamma'_1} \tag{53}$$

$$m'_{2c} = \frac{1}{\sin\gamma'_2} \tag{54}$$

whereas gear-to-blade rolls are set to

$$m'_{1b} = \frac{1}{\sin\gamma'_1} \cdot \frac{r_{ck}\sin\nu_k}{A_m\cos\psi_m}, \quad k = (i, o) \tag{55}$$

$$m'_{2b} = \frac{1}{\sin\gamma'_2} \cdot \frac{r_{ck}\sin\nu_k}{A_m\cos\psi_m}, \quad k = (i, o) \tag{56}$$

Besides, wheel axial error ΔA_2 will provide a new value for the machine center to back ΔX_{D2}

$$\Delta X_{D2} = \Delta A_2 \tag{57}$$

whereas the pinion axial error ΔA_1 and the shortest center distance error ΔE provides new values for the machine center to back ΔX_{D1} and the pinion blank offset ΔE_{m1}

$$\Delta X_{D1} = \Delta A_1 \tag{58}$$

$$\Delta E_{m1} = \Delta E \tag{59}$$

The proposed procedure for compensation of errors of alignment keeps the settings for the cutter such as inner and outer machine distances and inner and outer cradle angles as unmodified. The advantage is that such settings can be reserved for tooth thickness and backlash control through the additional slope angles of pinion and gear, and for lengthwise mismatch of pinion and gear tooth surfaces through the cutter radii.

5. Computerized simulation of meshing and contact. Numerical examples.

Simulation of meshing and contact of pinion and gear tooth surfaces is performed through a general purpose algorithm for tooth contact analysis (TCA). It is based on a numerical method that takes into account the position of the tooth surfaces and minimize the distances until contact is achieved, regardless of the type of contact (linear, point, or edge contact). The algorithm assumes rigid body behavior of tooth surfaces and is based on the work [22] and applied later in the works [23, 24]. Three pairs of teeth, two cycles of meshing, and a virtual compound thickness of

0.0065 mm have been used for determination of contact patterns and functions of transmission errors for all examples shown below. A total of 21 contact positions along the two cycles of meshing have been considered.

Simulation of backlash of the gear drive is based on: (i) computation of contact on one side of the gear tooth surfaces based on the previous algorithm, and (ii) computation of rotational backlash of the gear until contact is achieved in the opposite side of the gear tooth surfaces while the pinion is held at rest for each given contact position. The process is repeated for the same chosen number of contact positions than for TCA and considering three pairs of teeth and two cycles of meshing. Simulation of backlash allows backlash evolution analysis and interference detection even when errors of alignment are present. The results can be expressed in terms of circumferential backlash by multiplication of the rotational backlash and the outer pitch radius of the gear.

Geometry comparison analysis is based on computation of the distances between two chosen gear tooth surfaces, called primary and secondary geometries. The distances are measured along the normal at each point of a regular grid of points on one of the gear tooth surfaces, the primary geometry, and from such a point to the intersection point of the normal and the other gear tooth surface, the secondary geometry. Geometry comparison can be performed either considering the same rim angular position for both geometries or forcing the contact on one side (concave or convex) of the gear tooth surfaces.

The numerical examples are organized as follows:

(i) Determination of basic machine-tool settings from basic transmission data.

(ii) Advantages of the additional slope angle to control tooth thickness and backlash.

(iii) Adjusting the bearing contact in the cyclo-palloid system.

(iv) Compensating errors of alignment.

5.1. Determination of basic machine-tool settings from basic transmission data

The basic transmission data for a spiral bevel gear drive and the basic cyclo-palloid cutter data are represented in Table 1.

Table 1: Basic transmission and cyclo-palloid cutter data.

Data	Value
Reference gear ratio	2.5
Shaft angle [degrees]	90.0
Input power [KW]	100.0
Pinion speed [rpm]	2000.0
AGMA quality number	8
Cutter radius [mm]	75.0
Number of blade groups	5

Application of Standard ANSI/AGMA 2005-C96 allows blank data to be determined as it is shown in Table 2 for pinion and gear. Uniform tooth taper is assumed for gears produced through the cyclo-palloid system. This type of gears uses the mean normal module as reference instead of the outer transverse module. Table 2 shows as well the minimum normal backlash and the mean normal chordal tooth thicknesses that are required according to the calculations based on the mentioned standard. The minimum normal backlash B is measured at the outer cone. The results of basic machine-tool settings are represented in Table 3. The same radii for inner and outer blades were considered, $r_{ci} = r_{co} = 75$ mm. An slope angle of $\nu = 6.502314$ degrees with additional slope angles $\Delta\nu_1 = 0.103669$ degrees and $\Delta\nu_2 = 0.078489$ degrees were obtained according to the procedure described in Section 3.

Figure 11 shows the corresponding gear drive and the results of application of TCA when the convex side of the pinion tooth surfaces acts as driving surface. It is observed linear contact since the same radii for outer and inner blades were applied. The evolution of circumferential backlash along 21 contact positions is also illustrated in Fig. 11. A value about $B_c \approx 212.0\ \mu$m is obtained. Here, the circumferential backlash is evaluated considering

Table 2: Blank data.

Blank Data	Pinion	Gear
Tooth number	$N_1 = 16$	$N_2 = 41$
Pitch angle [degrees]	$\gamma_1 = 21.318$	$\gamma_2 = 68.682$
Spiral angle [degrees]	$\psi_m = 35.0$	
Hand of spiral	left-hand	right-hand
Outer transverse module [mm]	$m_{ot} = 4.874$	
Mean normal module [mm]	$m_{mn} = 3.397$	
Mean cone distance [mm]	$A_m = 91.265$	
Face width [mm]	$F_w = 32.0$	
Outer addendum [mm]	$a_{01} = 3.397$	$a_{02} = 3.397$
Outer dedendum [mm]	$b_{01} = 4.076$	$b_{02} = 4.076$
Face cone angle [degrees]	$\gamma_{F1} = 21.318$	$\gamma_{F2} = 68.682$
Root cone angle [degrees]	$\gamma_{R1} = 21.318$	$\gamma_{R2} = 68.682$
Minimum normal backlash [mm]	$B = 0, 150$	
Mean normal chordal addendum [mm]	$a_{c1} = 3.497$	$a_{c2} = 3.412$
Mean normal chordal tooth thickness [mm]	$t_{n1} = 5.271$	$t_{n2} = 5.276$

Table 3: Basic machine-tool settings for a gear drive with linear contact and given backlash.

Basic Machine-Tool Settings	Pinion	Gear
Inner machine distance [mm]	$M_{di} = 86.280818$	$M_{di} = 86.250146$
Inner cradle angle [degrees]	$q_{2i} = 49.878687$	$q_{2i} = 49.886702$
Outer machine distance [mm]	$M_{do} = 86.280818$	$M_{do} = 86.250146$
Outer cradle angle [degrees]	$q_{2o} = 49.878687$	$q_{2o} = 49.886702$
Machine center to back [mm]	$\Delta X_{D1} = 0.0$	$\Delta X_{D2} = 0.0$
Blank offset [mm]	$\Delta E_{m1} = 0.0$	$\Delta E_{m2} = 0.0$
Sliding base [mm]	$\Delta X_{B1} = 0.0$	$\Delta X_{B2} = 0.0$
Machine root angle [degrees]	$\gamma_{m1} = 21.318$	$\gamma_{m2} = 68.682$
Gear-to-cradle roll ratio	$m_{1c} = 2.750710$	$m_{2c} = 1.073448$
Gear-to-blade roll ratio	$m_{1b} = 0.317460$	$m_{2b} = 0.123417$

the outer pinion pitch radius. It cannot be directly compared with B since circumferential backlash is obtained in transverse section. However, $B_c \cdot \cos\psi_o$ will be close to B, where ψ_o is the outer spiral angle. On the other hand, the function of transmission errors is zero due to the conjugated action between pinion and gear tooth surfaces. Similar results will be obtained if opposite rotation of the pinion is provided.

5.2. Advantages of the additional slope angle to control tooth thickness and backlash

In case that the additional slope angles $\Delta\nu_1$ and $\Delta\nu_2$ are not applied, the gear drive will be provided with zero backlash. Figure 12 shows the results of geometry comparison between a pinion tooth surface provided with the additional slope angle $\Delta\nu_1 = 0.103669$ degrees, Σ_ν, and a pinion tooth surface without additional slope angle, Σ_g. Both surfaces are kept almost parallel each other as it is shown in Fig. 12(a). Figure 12(b) shows how close are both surfaces when contact between them is forced. The advantage of the additional slope angle $\Delta\nu_g$, $g = (1, 2)$, is that surface Σ_ν is very close to surface Σ_g, but shifted respect to it (as it is shown in Fig. 12(a)) for the purpose of tooth thickness and backlash control.

Another way to provide backlash is by making different the radii for inner and outer blades. Suppose that no additional slope angles are provided and cutter radii are set as $r_{ci} = 75.0$ mm and $r_{co} = 76.8$ mm for the pinion

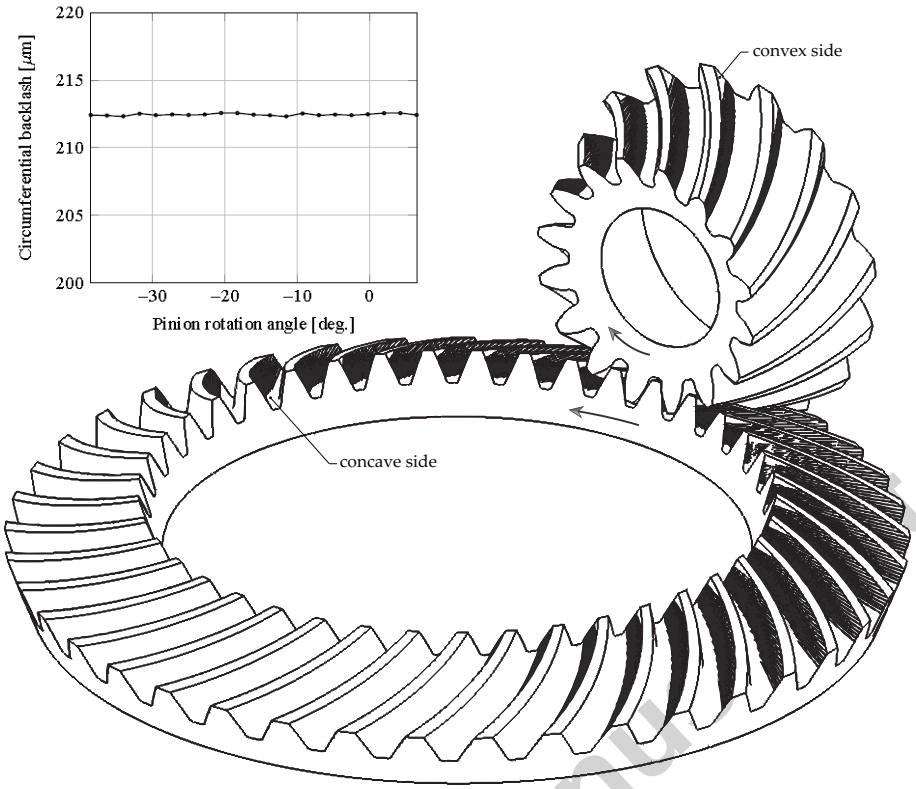

Figure 11: Contact pattern on the convex sides of the pinion tooth surfaces and the concave sides of the gear tooth surfaces and evolution of circumferential backlash.

generation. However, the radii are kept unmodified ($r_{ci} = r_{co} = 75.0$ mm) for the gear generation. The basic machine-tool settings for such arrangement are shown in Table 4.

Results of TCA for such a gear drive provide linear contact on the convex side of the pinion tooth surfaces and a zero level for the function of transmission errors similar to the results shown in Fig. 11. However, the linear contact is sacrificed on the concave sides of the pinion tooth surfaces as it is shown in Fig. 13. A contact pattern directed along the profile direction is observed as a consequence of the different cutter radii. A similar evolution of circumferential backlash is observed.

Therefore, the advantages of application of additional slope angles are evident due to the possibility to reserve cutter radii just for the functionality to adjust the bearing contact whereas the control and final adjustment of tooth thickness and backlash will depend exclusively on the additional slope angles.

5.3. Adjusting the bearing contact in the cyclo-palloid system

Although linear contact represents a preferable solution for reducing contact and bending stresses due to the uniform distribution of the load on the tooth surfaces, the truth is that such a type of contact is very sensitive to errors of alignment. The cyclo-palloid system provides a procedure to adjust the formation of the bearing contact through the longitudinal and profile crowning of the tooth surfaces. Whereas different cutter radii may be employed for longitudinal crowning of the tooth surfaces, application of different parabola coefficients a_p of the blade profiles (see Subsection 2.1) can be used for profile crowning. However, application of just profile crowning will result in a longitudinal bearing contact that is also very sensitive to errors of alignment.

A parabola coefficient $a_p = 0.0015$ mm$^{(-1)}$ for the blades that generate the pinion tooth surfaces is considered whereas straight profiles are considered for gear generation. Cutter radii $r_{ci} = 75.0$ mm and $r_{co} = 75.5$ mm for the inner and outer blades, respectively, are considered either for pinion generation or for gear generation. For these settings, additional slope angles $\Delta\nu_1$ and $\Delta\nu_2$ have to be determined for observation of tooth thicknesses shown in Table 2 and

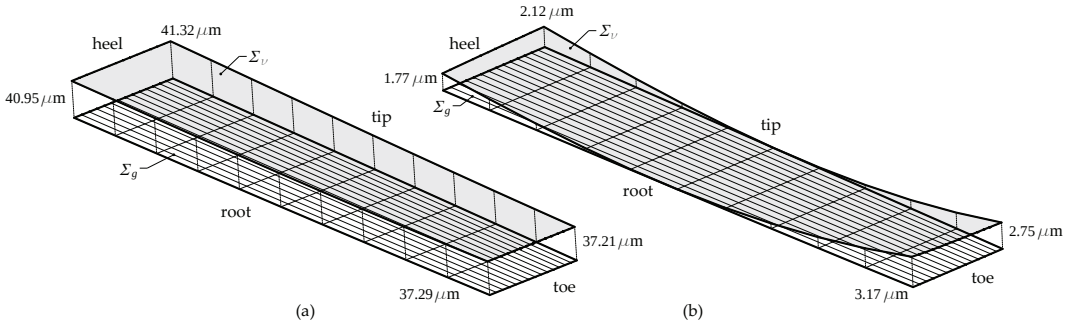

Figure 12: Geometry comparison between pinion tooth surfaces without slope modification, Σ_g, and with slope modification, Σ_v, for: (a) same rim angular position for the pinion tooth, (b) forcing contact between both surfaces.

Table 4: Basic machine-tool settings for pinion and gear with no additional slope angles and different cutter radii for pinion generation.

Basic Machine-Tool Settings	Pinion	Gear
Inner machine distance [mm]	$M_{di} = 86.154515$	$M_{di} = 86.154515$
Inner cradle angle [degrees]	$q_{2i} = 49.911665$	$q_{2i} = 49.991665$
Outer machine distance [mm]	$M_{do} = 86.638319$	$M_{do} = 86.154515$
Outer cradle angle [degrees]	$q_{2o} = 51.069306$	$q_{2o} = 49.911665$
Machine center to back [mm]	$\Delta X_{D1} = 0.0$	$\Delta X_{D2} = 0.0$
Blank offset [mm]	$\Delta E_{m1} = 0.0$	$\Delta E_{m2} = 0.0$
Sliding base [mm]	$\Delta X_{B1} = 0.0$	$\Delta X_{B2} = 0.0$
Machine root angle [degrees]	$\gamma_{m1} = 21.318$	$\gamma_{m2} = 68.682$
Gear-to-cradle roll ratio	$m_{1c} = 2.750710$	$m_{2c} = 1.073448$
Gear-to-blade roll ratio	$m_{1b} = 0.312500$	$m_{2b} = 0.121951$

following the procedure described in Section 3. The results are $\Delta\nu_1 = 0.052453$ degrees and $\Delta\nu_2 = 0.027427$ degrees. Basic machine-tool settings are shown in Table 5.

Figure 14 shows the contact pattern and backlash evolution for the gear drive with adjusted bearing contact. Results are represented on the concave side of the pinion tooth surfaces. Similar results are obtained for the convex side if pinion rotation is inverted. Figure 15 shows the function of transmission errors for such a gear drive. A maximum level of transmission errors of about 8 arcsec is observed.

5.4. Compensating errors of alignment

Errors of alignment may be caused by shaft deflections. Determination of errors of alignment due to shaft deflections in spiral bevel gear drives is described in [16] and is out of the scope of this paper. Here, we assumed as given such errors of alignment to prove the goodness of the approach proposed in Section 4. The following errors are considered: $\Delta E = 0.221$ mm, $\Delta A_1 = -0.005$ mm, $\Delta A_2 = 0.188$ mm, and $\Delta\gamma = -0.062$ deg. (see Fig. 9).

Figure 16 shows the results of TCA and backlash evolution for the gear drive with adjusted bearing contact when the above mentioned errors of alignment are present. The contact pattern is shifted towards the heel in the convex side of the pinion tooth surfaces and toward the toe in the concave side. The circumferential backlash is increased.

Basic machine-tool settings for the geometries that compensate the errors of alignment are determined following Section 4 and are represented in Table 6. The same additional slope angles are used here ($\Delta\nu_1 = 0.052453$ degrees and $\Delta\nu_2 = 0.027427$ degrees) than in previous subsection. Figure 17 shows the results of TCA for such a gear drive when no errors of alignment are present (no load is transmitted). It is observed that the formation of the bearing contact is not centered on the pinion tooth surfaces. Circumferential backlash has been decreased. However, as soon as the load is transmitted and the alignment errors appear, the bearing contact will be shifted towards a centered position on the tooth surfaces, as it is shown in Fig. 18. It is also observed that the circumferential backlash has been increased.

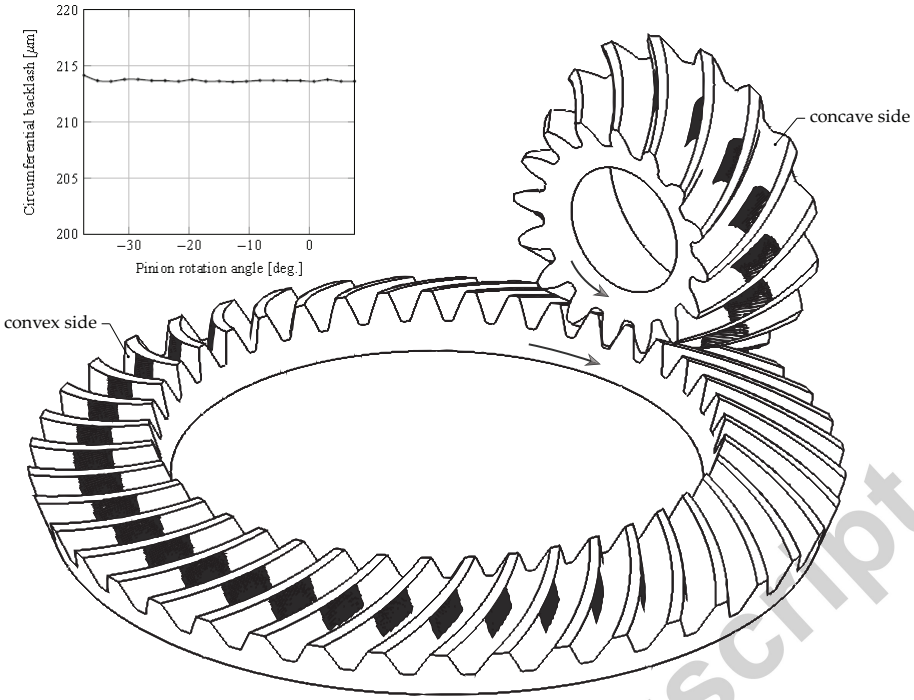

Figure 13: Contact pattern and backlash evolution at longitudinally mismatched pinion and gear tooth surfaces.

6. Conclusions

Based on the performed research work, the following conclusions can be drawn:

- A model for computerized generation of cyclo-palloid spiral bevel gears is presented. Such a model establishes the kinematic conditions when an additional slope angle is applied for tooth thickness and backlash control.
- An analytical approach for determination of basic-machine tool settings for generation of a cyclo-palloid spiral bevel gear drive with linear contact for both directions of rotation is presented. Tooth thicknesses for backlash control are guaranteed through a numerical method that determines the required additional slope angles.
- A method for adjusting the bearing contact in spiral bevel gear drives produced through the cyclo-palloid system is presented without losing sight of backlash control.
- An analytical approach for compensation of errors of alignment due to shaft deflections caused by a nominal load is presented.

Acknowledgements

The authors express their deep gratitude to the Spanish Ministry of Economy and Competitiveness (MINECO), for the financial support of research project ref. DPI2013-47702-C02-01 (financed jointly by FEDER).

References

[1] H. J. Stadtfeld, Cyclocut Bevel Gear Production, Gear Technology (2011) 36–49.
[2] S. Radzevich, Dudley's Handbook of Practical Gear Design and Manufacture, Second Edition, CRC Press, 2012.
[3] W. Krumme, Klingelnberg-Spiralkegelräder: Berechnung, Herstellung und Einbau, Springer-Verlag, Berlin and Heidelberg, 2013.
[4] M. Lelkes, J. Marialigeti, D. Play, Numerical Determination of Cutting Parameters for the Control of Klingelnberg Spiral Bevel Gear Geometry, Journal of Mechanical Design, Transactions of the ASME 124 (4) (2002) 761–771.

Table 5: Basic machine-tool settings for pinion and gear with an adjusted bearing contact.

Basic Machine-Tool Settings	Pinion	Gear
Inner machine distance [mm]	$M_{di} = 86.218428$	$M_{di} = 86.187936$
Inner cradle angle [degrees]	$q_{2i} = 49.894986$	$q_{2i} = 49.902945$
Outer machine distance [mm]	$M_{do} = 86.349162$	$M_{do} = 86.318731$
Outer cradle angle [degrees]	$q_{2o} = 50.217703$	$q_{2o} = 50.225748$
Machine center to back [mm]	$\Delta X_{D1} = 0.0$	$\Delta X_{D2} = 0.0$
Blank offset [mm]	$\Delta E_{m1} = 0.0$	$\Delta E_{m2} = 0.0$
Sliding base [mm]	$\Delta X_{B1} = 0.0$	$\Delta X_{B2} = 0.0$
Machine root angle [degrees]	$\gamma_{m1} = 21.318$	$\gamma_{m2} = 68.682$
Gear-to-cradle roll ratio	$m_{1c} = 2.750710$	$m_{2c} = 1.073448$
Gear-to-blade roll ratio	$m_{1b} = 0.315010$	$m_{2b} = 0.122463$

Table 6: Basic machine-tool settings for pinion and gear with an adjusted bearing contact and compensation of errors of alignment.

Basic Machine-Tool Settings	Pinion	Gear
Inner machine distance [mm]	$M_{di} = 86.218428$	$M_{di} = 86.187936$
Inner cradle angle [degrees]	$q_{2i} = 49.894986$	$q_{2i} = 49.902945$
Outer machine distance [mm]	$M_{do} = 86.349162$	$M_{do} = 86.318731$
Outer cradle angle [degrees]	$q_{2o} = 50.217703$	$q_{2o} = 50.225748$
Machine center to back [mm]	$\Delta X_{D1} = -0.005$	$\Delta X_{D2} = 0.188$
Blank offset [mm]	$\Delta E_{m1} = 0.221$	$\Delta E_{m2} = 0.0$
Sliding base [mm]	$\Delta X_{B1} = 0.0$	$\Delta X_{B2} = 0.0$
Machine root angle [degrees]	$\gamma_{m1} = 21.310$	$\gamma_{m2} = 68.628$
Gear-to-cradle roll ratio	$m_{1c} = 2.751720$	$m_{2c} = 1.073842$
Gear-to-blade roll ratio	$m_{1b} = 0.315125$	$m_{2b} = 0.122508$

[5] Y.-P. Shih, Z.-H. Fong, G. C. Y. Lin, Mathematical Model for a Universal Face Hobbing Hypoid Gear Generator, Journal of Mechanical Design, Transactions of the ASME 129 (1) (2007) 38–47.

[6] K. Kawasaki, I. Tsuji, Analytical and Experimental Tooth Contact Pattern of Large-Sized Spiral Bevel Gears in Cyclo-palloid System, Journal of Mechanical Design 132 (4) (2010) 041004–1–041004–8.

[7] I. Gonzalez-Perez, A. Fuentes, R. Ruiz-Orzaez, An Approach for Determination of Basic Machine-Tool Settings From Blank Data in Face-Hobbed and Face-Milled Hypoid Gears, Journal of Mechanical Design 137 (9) (2015) 093303.

[8] ANSI/AGMA 2005-C96, Design Manual of Bevel Gears, American Gear Manufacturers Association, 1500 King Street, Suite 201, Alexandria, Virginia 22314, 2005.

[9] J. H. Argyris, A. Fuentes, F. L. Litvin, Computerized Integrated Approach for Design and Stress Analysis of Spiral Bevel Gears, Computer Methods in Applied Mechanics and Engineering 191 (11-12) (2002) 1057–1095.

[10] J. Achtmann, G. Bar, Optimized Bearing Ellipses of Hypoid Gears, Journal of Mechanical Design, Transactions of the ASME 125 (4) (2003) 739–745.

[11] P.-Y. Wang, Z.-H. Fong, Fourth-Order Kinematic Synthesis for Face-Milling Spiral Bevel Gears With Modified Radial Motion (MRM) Correction, Journal of Mechanical Design 128 (2) (2006) 457.

[12] Q. Fan, Tooth Surface Error Correction for Face-Hobbed Hypoid Gears, Journal of Mechanical Design 132 (1) (2010) 011004.

[13] A. Artoni, M. Gabiccini, M. Guiggiani, A. Kahraman, Multi-Objective Ease-Off Optimization of Hypoid Gears for Their Efficiency, Noise, and Durability Performances, Journal of Mechanical Design 133 (12) (2011) 121007.

[14] H. Tamura, K. Kawasaki, Y. Nakano, Method for inspection of spiral bevel gears in klingelnberg cyclo-palloid system, JSME international journal. Ser. C, Dynamics, control, robotics, design and manufacturing 39 (1) (1996) 102–107.

[15] I. Gonzalez-Perez, V. Roda-Casanova, A. Fuentes, Modified geometry of spur gear drives for compensation of shaft deflections, Meccanica 50 (7) (2015) 1855–1867.

[16] A. Fuentes, R. Ruiz-Orzaez, I. Gonzalez-Perez, Compensation of errors of alignment caused by shaft deflections in spiral bevel gear drives, Vol. 34, Springer International Publishing, 2016.

[17] D. Vecchiato, Computerized Design , Simulation of Face-Hobbed Hypoid Gears , and Tooth Contact Analysis of Loaded Gear Drives By Boundary Element Method, Ph.D. thesis, University of Illinois at Chicago (2004).

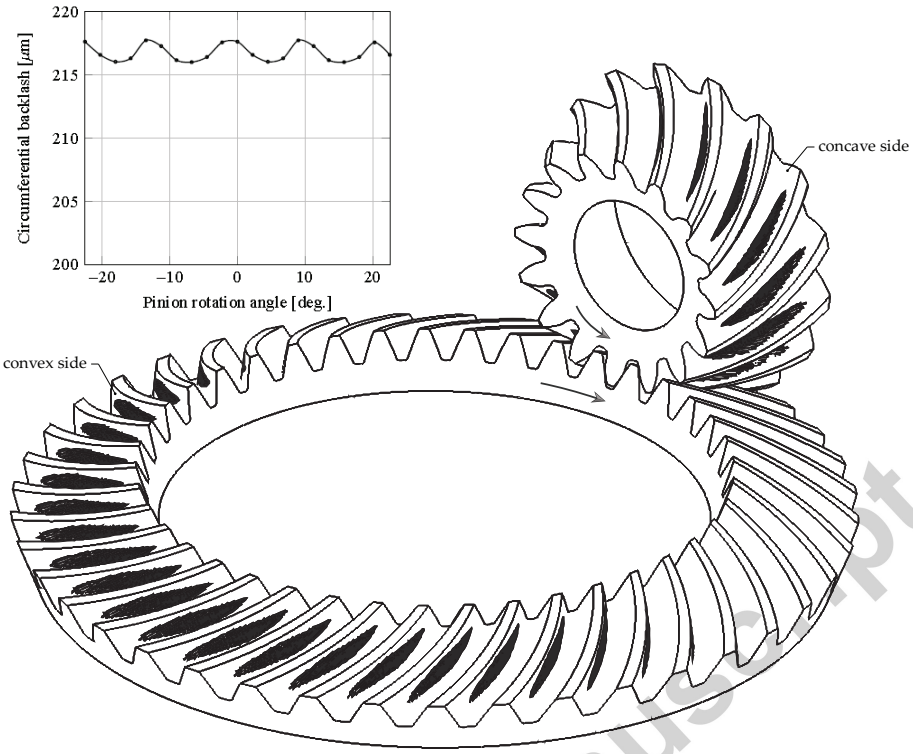

Figure 14: Contact pattern and backlash evolution for a gear drive with adjusted bearing contact.

[18] Q. Fan, Computerized Modeling and Simulation of Spiral Bevel and Hypoid Gears Manufactured by Gleason Face Hobbing Process, Journal of Mechanical Design 128 (6) (2006) 1315–1327.
[19] M. Vimercati, Mathematical model for tooth surfaces representation of face-hobbed hypoid gears and its application to contact analysis and stress calculation, Mechanism and Machine Theory 42 (6) (2007) 668–690.
[20] F. Litvin, A. Fuentes, Gear Geometry and Applied Theory, Second Edition, Cambridge University Press, New York, 2004.
[21] Y. Jaluria, Computer Methods for Engineering, Taylor & Francis, New York, 1996.
[22] G. I. Sheveleva, A. E. Volkov, V. I. Medvedev, Algorithms for analysis of meshing and contact of spiral bevel gears, Mechanism and Machine Theory 42 (2) (2007) 198–215.
[23] A. Fuentes, J. L. Iserte, I. Gonzalez-Perez, F. T. Sanchez-Marin, Computerized design of advanced straight and skew bevel gears produced by precision forging, Computer Methods in Applied Mechanics and Engineering 200 (29-32) (2011) 2363–2377.
[24] A. Fuentes, R. Ruiz-Orzaez, I. Gonzalez-Perez, Computerized design, simulation of meshing, and finite element analysis of two types of geometry of curvilinear cylindrical gears, Computer Methods in Applied Mechanics and Engineering 272 (2014) 321–339.

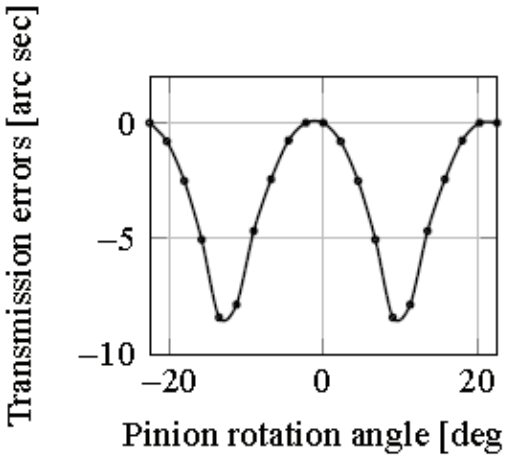

Figure 15: Function of transmission errors for a gear drive with adjusted bearing contact.

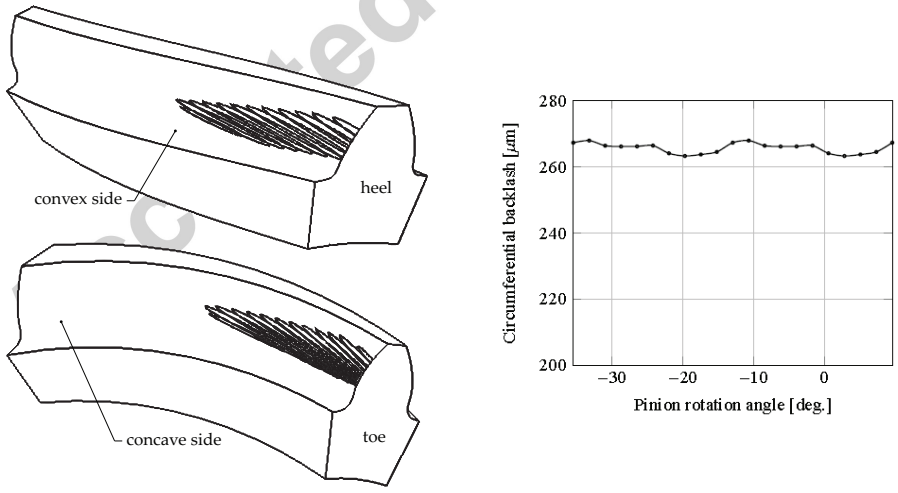

Figure 16: Contact pattern on both sides of pinion tooth and backlash evolution for a misaligned gear drive with adjusted bearing contact.

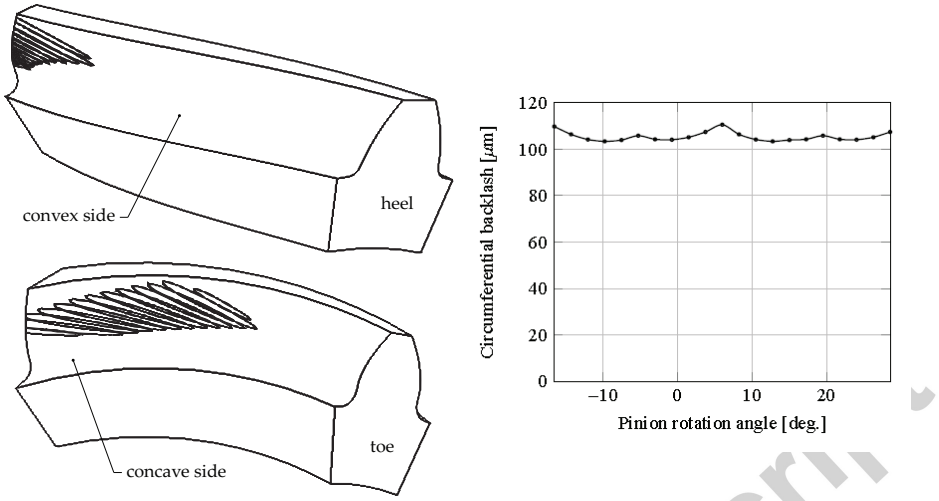

Figure 17: Contact pattern on both sides of pinion tooth and backlash evolution for an aligned gear drive with adjusted bearing contact and errors compensation.

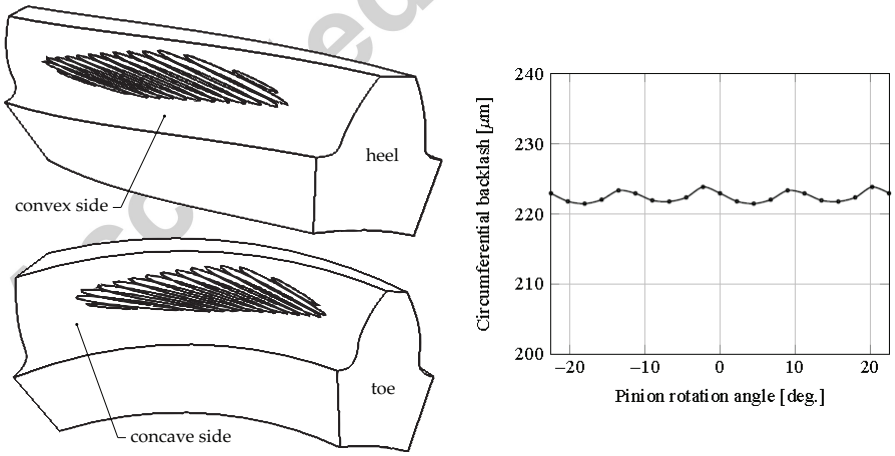

Figure 18: Contact pattern on both sides of pinion tooth and backlash evolution for a misaligned gear drive with adjusted bearing contact and errors compensation.